Draft version October 10, 2005
Preprint typeset using LaTeX style emulateapj v. 10/10/03

SOLAR DIFFERENTIAL ROTATION INFLUENCED BY LATITUDINAL ENTROPY VARIATIONS IN THE TACHOCLINE

Mark S. Miesch
High Altitude Observatory, NCAR[1], Boulder, CO 80307-3000

Allan Sacha Brun
DSM/DAPNIA/SAp, CEA Saclay, Gif sur Yvette, 91191 Cedex, France

Juri Toomre
JILA and Dept. Astrophysical & Planetary Sciences, University of Colorado, Boulder, CO 80309-0440
Draft version October 10, 2005

ABSTRACT

Three-dimensional simulations of solar convection in spherical shells are used to evaluate the differential rotation that results as thermal boundary conditions are varied. In some simulations a latitudinal entropy variation is imposed at the lower boundary in order to take into account the coupling between the convective envelope and the radiative interior through thermal wind balance in the tachocline. The issue is whether the baroclinic forcing arising from tachocline-induced entropy variations can break the tendency for numerical simulations of convection to yield cylindrical rotation profiles. As the amplitude of the imposed variation is increased, cylindrical rotation profiles do give way to more solar-like (conical) profiles which exhibit nearly radial angular velocity contours at mid-latitudes. Non-cylindrical rotation profiles are maintained primarily by the resolved convective heat flux which transmits entropy variations from the lower boundary into the convective envelope, giving rise to baroclinic forcing. The relative amplitude of the imposed entropy variations is of order 10^{-5}, corresponding to a latitudinal temperature variation of about 10K. The role of thermal wind balance and tachocline-induced entropy variations in maintaining the solar differential rotation is discussed.

Subject headings: Convection, Sun:rotation, Sun:interior, Tachocline

1. INTRODUCTION

One of the triumphs of helioseismology in the past two decades has been the determination of the solar internal rotation profile through the frequency splittings of global acoustic oscillations (Thompson et al. 2003). A striking feature of the inferred rotation profile is the nearly radial orientation of angular velocity contours at mid-latitudes; the angular velocity decreases monotonically from equator to pole by about 30% throughout the convective envelope. Near the base of the convective zone, there is a transition to approximately uniform rotation in the deep radiative interior across a boundary layer known as the tachocline.

The differential rotation of the solar envelope is maintained by turbulent convection. Three-dimensional numerical simulations of convection in rotating spherical shells have succeeded in reproducing the gross features of the solar rotation profile, including the strong decrease in angular velocity from equator to pole, but the rotation profiles in many simulations tend to be more cylindrical (angular velocity contours parallel to the rotation axis) than conical (radial angular velocity contours) (e.g. Gilman 1977, 1978; Glatzmaier 1984; Gilman & Miller 1986; Miesch et al. 2000; Elliott et al. 2000; Robinson & Chan 2001; Brun & Toomre 2002; Brun et al. 2004).

Electronic address: miesch@ucar.edu, sacha.brun@cea.fr, jtoomre@solarz.colorado.edu

[1] The National Center for Atmospheric Research is operated by the University Corporation for Atmospheric Research under sponsorship of the National Science Foundation

However, but for (Miesch et al. 2000), the three-dimensional simulations have not yet dealt explicitly with penetration of convection into the stable radiative zone below, nor examined how a tachocline of shear can be sustained there. The inclusion of such penetrative dynamics into the simulations may well influence the differential rotation realized in the bulk of the convection zone, but computational challenges in resolving decelerating plumes and gravity waves have delayed addressing these questions. Yet we can estimate that the presence of the tachocline boundary layer of rotational shear at the base of the convection zone, as deduced from helioseismology, implies that latitudinal gradients of entropy are likely to exist there as part of thermal wind balance in that region. This motivates us to conduct new simulations of convection in the bulk of the zone to examine modifications to the differential rotation achieved from imposing latitudinal entropy gradients at the lower boundary that may be in rough accord with the presence of a tachocline deeper down.

The tendency for many of the convection simulations to produce cylindrical rotation profiles can be understood by considering the equation of momentum conservation for a rotating fluid. If Reynolds stresses, Lorentz forces, and viscous dissipation are small relative to Coriolis forces, and if a steady state is assumed, this equation reduces to geostrophic and hydrostatic balance. Under these conditions, we may derive the following expression (Kitchatinov & Rüdiger 1995; Durney 1999; Elliott et al. 2000; Brun & Toomre 2002; Thompson et al. 2003; Mi-

esch 2005)

$$\frac{\partial \langle S \rangle}{\partial \theta} = \frac{2C_P}{g}\, r^2 \sin\theta\, \mathbf{\Omega_0 \cdot \nabla} \Omega = \frac{2rC_P}{g}\, \mathbf{\Omega_0 \cdot \nabla} \langle v_\phi \rangle \quad , \tag{1}$$

with S the specific entropy, $\Omega(r,\theta)$ the mean angular velocity, C_P the pressure specific heat, g the gravitational acceleration, and v_ϕ the longitudinal component of the velocity relative to the rotating frame. Angular brackets $<>$ denote averages over longitude and time. A spherical polar coordinate system is implied with colatitude θ and radius r, rotating at a constant angular velocity $\mathbf{\Omega_0}$.

Equation (1) reflects a balance between Coriolis forces and the baroclinic term in the zonal component of the vorticity equation (§4). In the absence of latitudinal entropy gradients ($\partial \langle S \rangle / \partial \theta = 0$), it implies cylindrical rotation profiles such that $\mathbf{\Omega_0 \cdot \nabla} \Omega = 0$. This is a manifestation of the well-known Taylor-Proudman theorem for rotating fluids (e.g. Pedlosky 1987). Cylindrical profiles may be avoided either through baroclinic forcing ($\partial \langle S \rangle / \partial \theta \neq 0$) or through Reynolds stresses and Lorentz forces of sufficient amplitude to upset the balance expressed by equation (1).

If equation (1) applies and if $\partial \langle S \rangle / \partial \theta \neq 0$, then we say that the system is in thermal wind balance and we refer to the differential rotation Ω as a thermal wind. If this is the case, then a conical rotation profile in which the angular velocity decreases from low to high latitudes would be associated with an entropy variation which increases from low to high latitudes ($\partial \langle S \rangle / \partial \theta < 0$ in the northern hemisphere). Thus, if the solar differential rotation were in thermal wind balance, then we would expect the convection zone to possess relatively warm (large $\langle S \rangle$) poles.

Thermal wind balance has a long history in geophysical fluid dynamics (e.g. Pedlosky 1987) and its potential importance in connection with the solar differential rotation has been realized for decades (Plaskett 1959; Weiss 1965; Gilman 1968). Theoretical estimates of the amplitude of the Reynolds stresses within the context of mean-field models imply that they are weak relative to Coriolis forces, resulting in a balance as expressed by equation (1) (Kitchatinov & Rüdiger 1995; Durney 1996b, 1999; Rüdiger & Hollerbach 2004). Thus, recent mean-field models which produce solar-like (conical) rotation profiles generally do so by means of baroclinic forcing (Durney 2001; Küker & Stix 2001; Kitchatinov & Rüdiger 2005; Rempel 2005). Latitudinal entropy gradients in mean-field models are typically maintained by a latitudinally-dependent convective heat flux which is parameterized along with the Reynolds stresses as part of the turbulence model (Durney & Spruit 1979; Rüdiger et al. 2005).

In three-dimensional convection simulations a latitudinally-dependent convective heat flux arises naturally due to the influence of rotation on convective motions (Gilman 1977, 1978; Elliott et al. 2000; Brun & Toomre 2002). Depending on the parameter regime, this latitudinally-dependent convective heat flux can be considerable and can produce a substantial thermal wind differential rotation which is roughly conical in nature much as in the Sun (Elliott et al. 2000; Robinson & Chan 2001; Brun & Toomre 2002). However, these results are still sensitive to subgrid-scale dissipation models which are introduced in order to represent the influence of unresolved motions.

In order to break the Taylor-Proudman constraint, there must be a substantial poleward convective heat transport or substantial Reynolds stresses and Lorentz forces which would modify equation (1). In simulations and presumably also in the Sun, this is achieved mainly by the nonlinear advection of enthalpy, momentum, and magnetic flux in downflow plumes which represent the dominant coherent structures in turbulent compressible convection. It is unclear whether simulations currently have sufficient spatial resolution to fully capture the dynamics of such turbulent plumes. As the resolution of these models continues to increase and the influence of dissipation is reduced, the turbulent transport may be modified to more reliably produce solar-like (conical) rotation profiles.

An alternative or perhaps complementary possiblity is that thermal variations capable of breaking the Taylor-Proudman constraint originate partially in the tachocline. This has been suggested recently by Rempel (2005) within the context of a mean-field model. In Rempel's model, latitudinal entropy variations originate from meridional circulations in the subadiabatic portion of the tachocline and are then transmitted to the convective envelope by turbulent diffusion. This gives rise to a baroclinic forcing which breaks the Taylor-Proudman constraint and produces conical rotation profiles similar to the solar rotation profile inferred from helioseismology.

Baroclinic forcing in the convection zone induced by thermal coupling to the tachocline has not yet been investigated by means of three-dimensional convection simulations. Most global convection simulations to date do not incorporate convective penetration into the stably-stratified radiative interior. Rather, the lower boundary is placed at the base of the convective envelope in order to alleviate the computational difficulties associated with the overshoot region and tachocline. Such models have only considered latitudinally-uniform thermal boundary conditions which do not take into account possible dynamics occurring in the tachocline.

If the tachocline were in thermal wind balance, the strong rotational shear would imply relatively large latitudinal entropy variations according to equation (1). Thus, uniform thermal boundary conditions applied at the base of the convection zone in global simulations may not adequately reflect the coupling between the convection zone and the radiative interior via the tachocline, which lies outside of the computational domain. Motivated by Rempel's (2005) mean-field results and the importance of thermal wind balance in our previous work, we now consider the effects of applying a latitudinal entropy variation as a lower boundary condition to global-scale numerical simulations of solar convection. Our focus is the impact these modified boundary conditions have on the differential rotation profile in the convection zone. The numerical model and simulation strategy are described in §2 and results are reported in §3. In §4 we discuss in detail how thermal wind balance may arise in the solar tachocline, further justifying our choice of boundary conditions. Concluding remarks are offered in §5.

2. THE NUMERICAL MODEL

TABLE 1. SIMULATION SUMMARY

Case	a_2[a]	a_4[a]	CKE[b]	DRKE[b]	MCKE[b]
AB	...	...	2.3 (35%)	4.2 (64%)	0.022 (0.33%)
AB0	0	0	2.2 (45%)	2.7 (55%)	0.020 (0.41%)
AB1	1.0	0	2.2 (42%)	2.9 (57%)	0.022 (0.43%)
AB2	5.0	0	4.9 (57%)	3.7 (43%)	0.034 (0.40%)
AB3	2.7	- 0.43	2.8 (42%)	3.8 (58%)	0.026 (0.40%)

[a]Normalized by 10^{-6}. See eq. (2). In case AB $\partial S/\partial r$ is imposed rather than $S = S_b(\theta)$.

[b]Kinetic energy density relative to the rotating coordinate system decomposed into contributions from convection CKE, differential rotation DRKE, and meridional circulation MCKE, averaged over the full shell and over $\sim$ 300 days; units are 10^6 erg cm^{-3}.

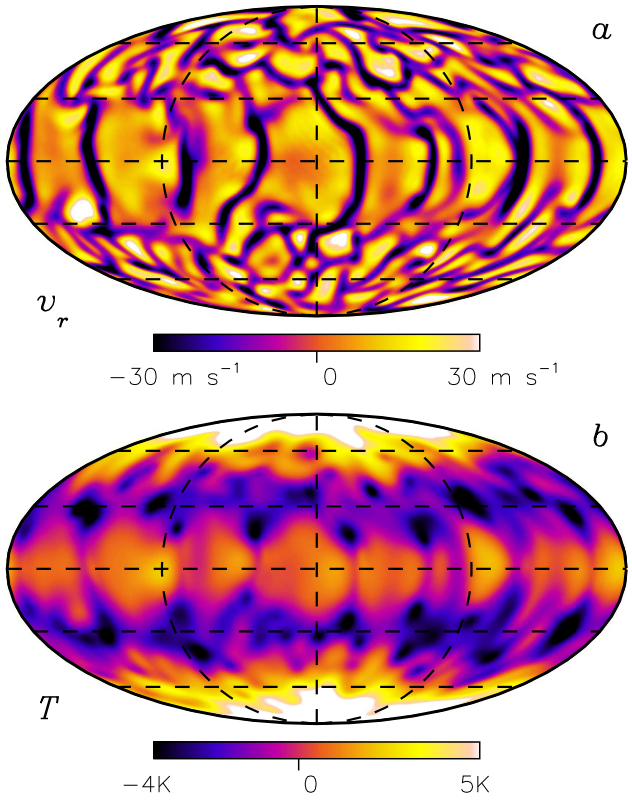

FIG. 1.— Snapshot of (a) the vertical velocity and (b) the temperature fluctuation near the top of the shell ($r = 0.95R_\odot$) in case AB3 (Mollweide projection). Yellow/white and blue/black tones denote upflow and downflow in (a) and warmer and cooler temperatures in (b) as indicated by the color tables. Dashed lines represent the latitude/longitude grid (spacing 30°/90°).

The simulations here were carried out using the ASH (Anelastic Spherical Harmonic) code described by Clune et al. (1999) and Brun et al. (2004). ASH is a pseudo-spectral code which employs spherical harmonic and Chebyshev basis functions and Adams-Bashforth/Crank-Nicolson time-stepping. The three-dimensional anelastic equations of motion are solved in a rotating spherical shell with a background stratification derived from a solar structure model.

The simulations here are variations of case AB, which has been defined and discussed by Brun & Toomre (2002). All (including case AB itself as a control) were initiated from the same AB restart files and evolved for over 100 rotation periods ($\sim$ 3000 days). The computational domain in radius spans 0.72–0.96$R_\odot$ and the number of grid points in latitude, longitude, and radius is in turn 128, 256, and 65. The velocity boundary conditions are stress-free and impenetrable. The subgrid-scale viscosity and diffusivity are $\nu = 2.8 \times 10^{12}$ cm^2 s^{-1} and $\kappa = 1.1 \times 10^{13}$ cm^2 s^{-1} respectively, implying a Prandtl number of $P_r = \nu/\kappa = 0.25$. Both κ and ν vary with radius as $\overline{\rho}^{-1}$, where $\overline{\rho}(r)$ is the mean density. The Rayleigh and Reynolds numbers near the middle of the convection zone are of order 3×10^4 and 10^2 respectively.

The difference between the five simulations reported here lies in the lower thermal boundary condition as summarized in Table 1. In case AB the radial entropy gradient is held constant at the inner boundary which fixes the subgrid-scale heat flux (Clune et al. 1999). This allows for latitudinal entropy variations to be established by convective heat transport (cf. Fig. 3) but does not impose such variations. The remaining simulations have an imposed latitudinal entropy profile of the form

$$\frac{S_b(\theta)}{C_P} = a_2 Y_2^0 + a_4 Y_4^0 \sim \frac{T}{\overline{T}} \quad , \qquad (2)$$

where S_b is the specific entropy at the base of the computational domain, T is the associated temperature variation, and $\overline{T}(r)$ is the mean temperature. Y_ℓ^m is a spherical harmonic of order ℓ and degree m. For the simulations here, $C_P = 3.5 \times 10^8$ erg g^{-1} K^{-1} and $\overline{T} \sim 2 \times 10^6$ K at the lower boundary. The upper thermal boundary condition in all cases is a fixed radial entropy gradient which results in a fixed, latitudinally-uniform heat flux through the upper surface.

The values of a_2 and a_4 are chosen such that the pole is warmer than the equator by 5-10K (Fig. 4). The sense and amplitude of this variation is consistent with the entropy gradient implied by equation (1) assuming an Ω profile as inferred from helioseismic inversions (Thompson et al. 2003). However, the amplitude of the entropy variation in the Sun is uncertain due to uncertainty in the rotational shear; the tachocline may well be narrower than can be resolved by helioseismic probing.

3. MODIFYING THE DIFFERENTIAL ROTATION

According to our previous simulations with the ASH code, those cases that produce the most solar-like rotation profiles also possess relatively large latitudinal entropy gradients (involving temperature variations of order 10 K) and exhibit thermal wind balance near the base of the convection zone (Elliott et al. 2000; Brun & Toomre 2002). A representive simulation which exhibits this quality is case AB of Brun & Toomre (2002). Latitudinal entropy gradients $\partial \langle S \rangle / \partial \theta$ are established by the resolved convective motions alone by means of a latitude-dependent heat flux. Such gradients are permitted but not imposed by the thermal boundary conditions which fix the radial entropy gradient $\partial S/\partial r$. Thermal wind balance is broken in the upper convection zone where Reynolds stresses and viscous diffusion are responsible for the non-cylindrical angular velocity contours ($\boldsymbol{\Omega_0 \cdot \nabla \Omega} \neq 0$).

The purpose of this paper is to investigate whether

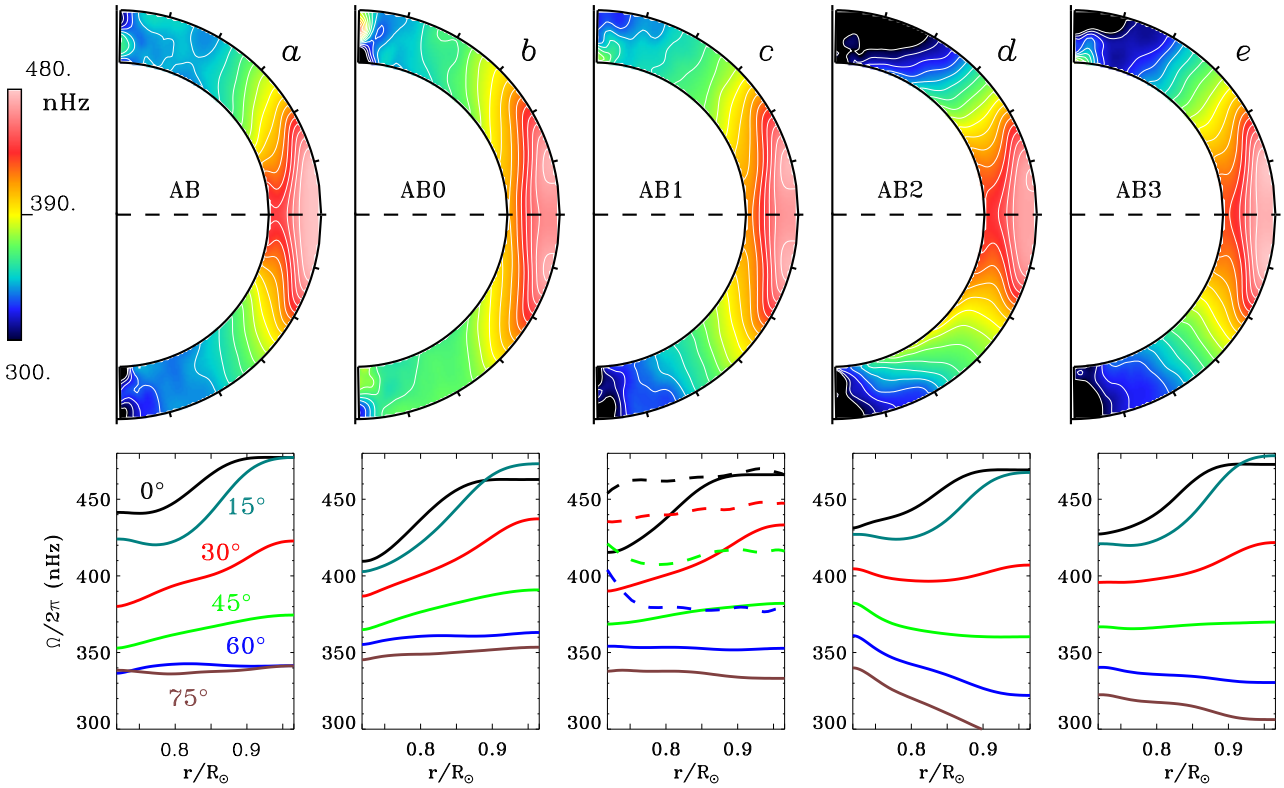

FIG. 2.— Angular velocity profiles $\Omega(r,\theta)$ for each simulation, averaged over longitude and time ($\sim$ 300 days). (Upper panels) Ω in the meridional plane with contours ranging from 310–470 nHz in steps of 10 nHz. (Lower panels) Radial profiles at selected latitudes as labelled. The Ω profile is most conical in case AB3. Helioseismic rotational inversions are shown in (*c*) for comparison (dashed lines), obtained by a SOLA inversion of SOHO/MDI data (Schou et al. 2002); the 15° curve there has been omitted for clarity.

tachocline-induced entropy variations can enhance the baroclinic forcing of the differential rotation which is already established by the latitude-dependent convective heat flux. Thus, we have taken case AB as a starting point and have imposed a latitudinal entropy variation on the bottom boundary as described in §2. Further justification for these boundary conditions is given in §4. In this section we present our primary results.

The convective flow structure in all cases is similar and is illustrated in Figure 1*a*. If the imposed entropy variation is weak, the kinetic energy in the differential rotation DRKE increases steadily with the amplitude of the variation with little effect on the convection kinetic energy CKE (cases AB0, AB1, AB3 in Table 1). As the imposed entropy variation is increased further (case AB2), it begins to influence the convective motions and CKE increases more rapidly than DRKE. The influence of the thermal boundary condition is more noticable in the temperature field (Fig. 1*b*). Those simulations with a relatively large imposed entropy varation (Cases AB2 and AB3) exhibit relatively warm poles throughout the convection zone. We will discuss this further below (see Figs. 3 and 4).

The mean differential rotation profile in each simulation is shown in Figure 2. The sequence of cases AB0–AB1–AB2 represents a progressive increase in amplitude of an imposed $\ell = 2$ entropy variation on the lower boundary from 0 to 10^{-6} to 5×10^{-6}. This produces a systematic transition from cylindrical to conical rotation profiles. Case AB3 (Fig. 2*e*) includes a contribution from the $\ell = 4$ spherical harmonic mode and also exhibits a conical rotation profile.

The solar rotation profile inferred from helioseismic inversions is plotted in Figure 2*c* for comparison (dashed lines). The angular velocity contrast $\Delta\Omega$ between the equator and latitudes of 60° is larger in the simulations ($\Delta\Omega/(2\pi) \sim$ 100–130 nHz) than in the Sun ($\Delta\Omega/(2\pi) \sim$ 90 nHz). However, the monotonic decrease in angular velocity with latitude and the conical nature of the solar profile, reflected in the small variation of the angular velocity with radius at mid-latitudes, is roughly captured by simulations AB2 and AB3. These are significantly more solar-like than the rotation profile in case AB (Fig. 2*a*) which does not include an imposed latitudinal entropy variations on the lower boundary. All simulations reported here are relatively laminar, non-magnetic, and non-penetrative. Turbulent transport, magnetism, and convective overshoot all tend to reduce $\Delta\Omega$ so we expect more sophisticated simulations to exhibit smaller, possibly more solar-like angular velocity contrasts (Miesch et al. 2000; Brun & Toomre 2002; Brun et al. 2004).

Gilman & Howe (2003) argue that Ω contours from helioseismic inversions at low and mid latitudes, though nearly radial, may be better interpreted as having a roughly constant angle with the rotation axis of $\sim 25°$. Simulations AB2 and AB3 have a similar property as can

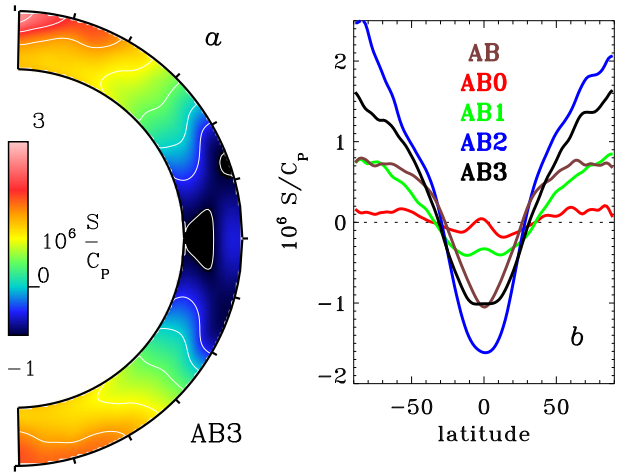

FIG. 3.— (*a*) Mean entropy profile in case AB3, averaged over longitude and time. Colors and contours (spacing 0.5) show relative variation $10^6 S/C_P$. (*b*) Latitudinal variation of mean entropy at mid-depth ($r = 0.84 R_\odot$) for all cases.

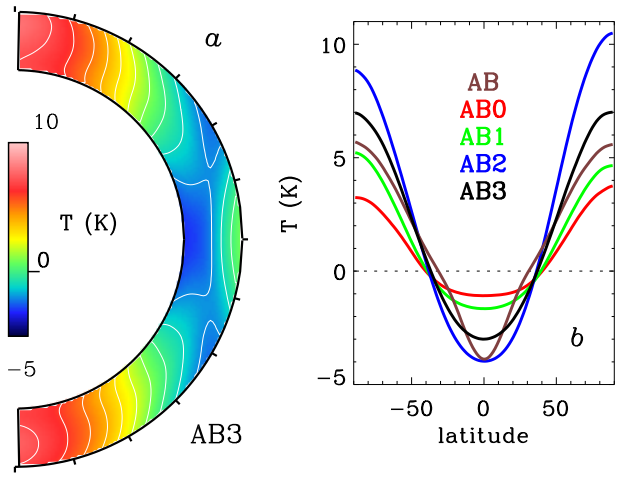

FIG. 4.— (*a*) Mean temperature profile in case AB3, averaged over longitude and time. Colors and contours (spacing 1K) represent temperature variations. (*b*) Latitudinal variation of mean temperature at the lower boundary ($r = 0.72 R_\odot$) for all cases.

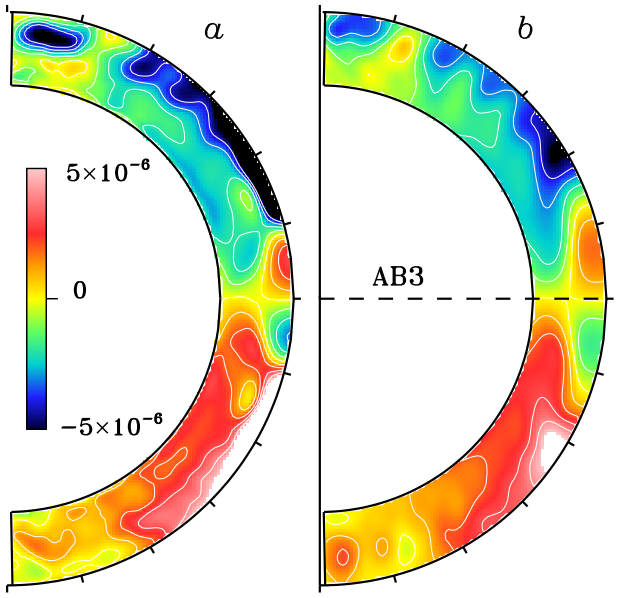

FIG. 5.— (*a*) $2rg^{-1}\mathbf{\Omega_0}\cdot\nabla v_\phi$ and (*b*) $C_P^{-1}\partial\langle S\rangle/\partial\theta$ for case AB3, averaged over longitude and time. Correspondence between (*a*) and (*b*) indicates thermal wind balance as expressed by equation (1). Each quantity is dimensionless and contour levels are spaced at 10^{-6}.

be verified from Figures 2*d*,*e*.

Conical rotational profiles in our simulations are clearly associated with latitudinal entropy variations, as demonstrated in Figure 3*a*, suggesting that thermal wind balance plays an important role. The entropy variation in Case AB is intermediate between cases AB0 and AB2. Here a latitudinal entropy gradient is allowed by the lower boundary condition but it is not imposed. Convection redistributes entropy and angular momentum such that thermal wind balance is maintained in the lower convection zone but the resulting entropy variations are not as large as in case AB2.

The sense of the imposed entropy gradient is such that the poles are relatively warm (high-entropy). In thermal wind balance, this implies a negative (positive) value of $\mathbf{\Omega_0}\cdot\nabla\Omega$ in the northern (southern) hemisphere as expressed by equation (1). If the imposed entropy variation is weak, much of this rotational shear is manifested in the latitudinal component of the differential rotation which exhibits a monotonic decrease in angular velocity toward the poles throughout the convection zone as in case AB1. As the amplitude of the variation is increased, radial gradients in Ω are established at high latitudes where the rotation vector is nearly vertical. If an $\ell = 4$ component is included in the boundary condition then the high-latitude radial shear may be reduced while still maintaining nearly radial angular velocity contours at mid-latitudes. This is demonstrated by case AB3 which represents our most solar-like rotation profile. Rotation and entropy profiles for case AB3 are shown in Figures 2 and 3.

The thermal boundary condition is applied to the entropy field but its signature is also apparent in the temperature field (Fig. 4). The pole-equator temperature difference in cases AB2 and AB3 is about 10K. It is remarkable that this relatively small variation is enough to have a substantial influence on the differential rotation profile (Fig. 2).

The role of baroclinic forcing in maintaining the conical rotation profile in cases AB2 and AB3 can be addressed by comparing the left and right-hand sides of equation (1). If these are equal then the system is in thermal wind balance and non-cylindrical rotation profiles are associated with latitudinal entropy gradients. The degree to which this applies in case AB3 is illustrated in Figure 5. Thermal wind balance is approximately satisfied in the lower convection zone but significant departures exist in the upper convection zone where Reynolds stresses are no longer neglible. Similar assessments hold for the other simulations presented here and in previous work (Elliott et al. 2000; Robinson & Chan 2001; Brun & Toomre 2002).

The amplitude and profile of the mean entropy vari-

ation in the solar tachocline is unknown. Helioseismic structure inversions are sensitive to broad thermal variations of $S/C_P \gtrsim 10^{-5}$ (Antia et al. 2003), which is likely not sufficient to detect the relatively weak, localized variations associated with thermal wind balance in the tachocline. If Ω profiles from current rotational inversions are translated into entropy gradients according to equation (1), this implies amplitudes $S/C_P \sim 5 \times 10^{-6}$, corresponding to a monotonic temperature increase of about 8K from equator to pole (Miesch 2005). This is a conservative estimate, as the width of the tachocline may well be narrower than the resolution of the inversion kernels, implying larger rotational gradients and thus larger thermal variations.

The computational domain in the simulations reported here only extends to $r = 0.96R_\odot$ and the heat flux through this outer surface is fixed and latitudinally uniform. However, if a latitudinal entropy variation were present in the solar convection zone, it might give rise to latitudinal variations in the temperature or irradiance at the level of the photosphere. The detection of such signatures is complicated by magnetic effects but photospheric observations indicate that relative latitudinal temperature variations are no larger than a few $\times 10^{-4}$ (Altrock & Canfield 1972; Kuhn et al. 1988; Woodard & Libbrecht 2003). The relative thermal variations shown in Figures 3 and 4 are well within these observational limits.

It is notable that the meridional circulation is not as sensitive to the lower thermal boundary condition. All simulations reported here exhibit multi-celled patterns similar to case AB (Brun & Toomre 2002) with comparable amplitudes as reflected by their kinetic energy content (Table 1). However, systematic differences between simulations are realized as shown in Figure 6. Those simulations in which a substantial latitudinal entropy variation is applied (cases AB2 and AB3) exhibit a narrow region of clockwise circulation near the lower boundary in the northern hemisphere (counter-clockwise in the southern hemisphere) which is either absent or less pronounced in cases AB and AB1. This reflects the mechanism by which thermal wind balance is established, as we will discuss presently in §4.

The meridional circulation near the surface of the Sun is generally poleward at latitudes $< 60^\circ$ with an amplitude of $\sim$ 15-20 m s^{-1}, but it fluctuates substantially over the course of months and years (Hathaway 1996; Snodgrass & Dailey 1996; Haber et al. 2002; Basu & Antia 2003; Zhao & Kosovichev 2004). Meridional circulation patterns deep in the solar convection zone are still unknown although some local helioseismic inversions have suggested that the poleward surface flow may persist down to $\sim 0.96R_\odot$ and possibly deeper (Giles et al. 1997; Braun & Fan 1998). Other inversions provide evidence for multi-cell structure. In particular, Haber et al. (2002) have reported a flow reversal several Mm below the photosphere in the northern hemisphere which lasted from 1998 until at least 2001.

The outer boundary of our simulation domain is placed at $0.96R_\odot$ so our results cannot be compared directly with meridional circulation patterns determined from photospheric measurements and local helioseismic inversions which generally focus on $r > 0.96R_\odot$. However, near-surface flows may persist deeper into the interior than can currently be observed. The meridional circulation near the outer boundary of our simulations is similar in amplitude and form to that determined from photospheric measurements and helioseismic inversions, though poleward flow in the simulations is generally confined to lower latitudes ($\lesssim 35^\circ$; see Fig. 6).

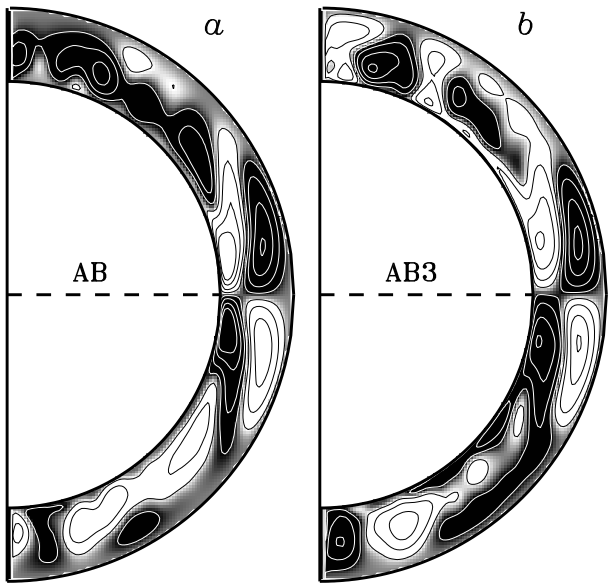

FIG. 6.— Streamlines of the mass flux in the meridional plane for cases (*a*) AB and (*b*) AB3, averaged over longitude and time. Black contour lines on a white background indicates clockwise circulation while white contour lines on a black background indicates counter-clockwise circulation.

The meridional circulation in the solar convection zone and tachocline has important implications for modeling the 11-yr solar activity cycle, particularly for mean-field dynamo models of the Babcock-Leighton type (reviewed by Charbonneau 2005). In many dynamo models, referred to as flux-transport models, the advection of magnetic flux by global circulations plays an essential role in many aspects of the activity cycle including the direction of field migration, the period of magnetic field reversals and the phase relationship between poloidal and toroidal fields (Durney 1996a; Dikpati & Charbonneau 1999; Küker et al. 2001; Nandy & Choudhuri 2002). These models are generally kinematic and assume a large-scale circulation pattern consisting of one cell per hemisphere, counter-clockwise in the north and clockwise in the south. Recent models have also begun to consider more complicated circulation patterns and have generally concluded that the flux-transport mechanism can still operate. Charbonneau & Dikpati (2000) introduced random stochastic fluctuations while Dikpati et al. (2004) and Bonnanno et al. (2005) considered multiple cells in latitude. Jouve & Brun (2006) are the first to develop Babcock-Leighton dynamo models with multi-celled circulation patterns in radius as well as latitude, much as in the convection simulations (Fig. 6). They find that such multi-celled patterns can significantly slow down the reversal period, requiring larger-amplitude meridional flows to achieve an 11-year cycle.

4. HOW MIGHT THERMAL WIND BALANCE BE ACHIEVED?

To the extent that Reynolds stresses and Lorentz forces may be neglected, equation (1) represents an equilibrium state. In order to determine the relevance of this equation to the solar tachocline and convection zone, we must ask whether this equilibrium is stable and whether it is likely to be achieved in practice. We shall argue here that thermal wind balance should be a robust feature of the tachocline and lower convection zone except in localized regions where it may be disrupted by strong magnetic fields.

Equation (1) is derived from the zonal component of the vorticity equation. If we retain the time derivative (while still neglecting Reynolds stresses, Lorentz forces, and viscous diffusion) we obtain (cf. Rempel 2005)

$$\frac{\partial \omega_\phi}{\partial t} = 2r\sin\theta \mathbf{\Omega_0}\cdot\boldsymbol{\nabla}\Omega - \frac{g}{rC_P}\frac{\partial \langle S\rangle}{\partial\theta} \qquad (3)$$

where ω_ϕ is the zonal component of the fluid vorticity relative to the rotating frame. In a steady state, equation (3) reduces to equation (1).

We now consider two possible ways in which an equilibrium may be reached which we will distinguish as shear-induced and thermally-induced. In the shear-induced case, we may assume that latitudinal entropy variations are initially zero $\partial\langle S\rangle/\partial\theta = 0$ but convective Reynolds stresses and perhaps other tachocline processes establish a shear $\mathbf{\Omega_0}\cdot\boldsymbol{\nabla}\Omega \neq 0$. We may then ask whether the induced circulations implied by equation (3) move the system toward thermal wind balance [eqn. (1)].

According to helioseismic inversions and numerical simulations, $\mathbf{\Omega_0}\cdot\boldsymbol{\nabla}\Omega$ is negative in the northern hemisphere (for simplicity we focus on the northern hemisphere - the sense of the circulations and the gradients is reversed in the southern hemisphere). Equation (3) then indicates that a counter-clockwise circulation ($\omega_\phi < 0$) would be induced as a consequence of the mechanical forcing which maintains the shear. This is related to the mechanism of gyroscopic pumping discussed by McIntyre (1998) and Gough & McIntyre (1998). In order to determine what effect this will have on the redistribution of entropy we must consider the energy equation:

$$\frac{\partial\langle S\rangle}{\partial t} = -\left\langle \boldsymbol{v}\cdot\boldsymbol{\nabla}\left(S+\overline{S}\right)\right\rangle + [\ldots] \sim -\langle v_r\rangle\frac{d\overline{S}}{dr} \qquad (4)$$

where $\overline{S}$ is the background (spherically-averaged) entropy within the anelastic approximation (e.g. Miesch 2005). In the convection zone $d\overline{S}/dr$ is negative. A counter-clockwise circulation (outward at the equator and inward at the poles) would then tend to warm the equator relative to higher latitudes, moving the system farther from the balance expressed by equation (1). However, in the subadiabatic tacholine ($d\overline{S}/dr > 0$), a counter-clockwise circulation induced by a solar-like rotational shear would warm the poles, tending to establish thermal wind balance (provided Reynolds stresses and Lorentz forces remain neglibible).

We now consider the thermally-induced case in which we begin with a latitudinal entropy gradient $\partial\langle S\rangle/\partial\theta \neq 0$ in the absence of shear $\mathbf{\Omega_0}\cdot\boldsymbol{\nabla}\Omega$ and we ask whether the induced circulation will tend to establish a differential rotational in accordance with equation (1). The answer is yes, for both a subadiabatic and a superadiabatic background stratification. To illustrate this, we consider the zonal momentum equation which may be written as

$$\frac{\partial\mathcal{L}}{\partial t} = -\langle\boldsymbol{v}\rangle\cdot\boldsymbol{\nabla}\mathcal{L} + [\ldots] \qquad (5)$$

where $\mathcal{L} = r\sin\theta\left(r\sin\theta\mathbf{\Omega_0} + \langle v_\phi\rangle\right)$ is the specific angular momentum density (Elliott et al. 2000). We neglect other contributions on the right-hand-side due to Reynolds stresses and Lorentz forces and we assume that our initial entropy profile possesses warm poles ($\partial\langle S\rangle/\partial\theta < 0$ in the northern hemisphere). We choose this profile because of its solar implications; similar arguments would apply to an arbritrary latitudinal entropy variation.

Warm poles would induce a clockwise meridional circulation in the northern hemisphere according to equation (3). If we begin with a cylindrical rotation profile such that $\boldsymbol{\nabla}\mathcal{L}$ is directed away from the rotation axis, then the effect of a global clockwise meridional circulation will be to decelerate the rotation rate in the upper convection zone and accelerate the lower convection zone where the flow is toward and away from the axis respectively. This would tilt angular velocity contours in a clockwise sense, tending to move the system toward thermal wind balance with a non-cylindrical rotation profile.

In summary, thermal forcing such as that maintained by latitudinally-dependent convective heat flux will induce circulations which will drive the system toward thermal wind balance but mechanical forcing will only do so in the subadiabatic tachocline. Once thermal wind balance is achieved, these circulations will cease unless other terms in equation (3) become important such as Reynolds stresses or Lorentz forces.

A subadiabatic tachocline is thus an essential component of Rempel's (2005) model discussed in §1. In his model, rotational shear is maintained by mechanical forcing which induces a counter-clockwise circulation through equation (3). A persistent counter-clockwise circulation is also present within the convection zone, maintained by Coriolis forces and Reynolds stresses. This convection-zone circulation penetrates downward, combining with tachocline-induced circulations to produce a net flow in the subadiabatic region which is downward at the poles and upward at the equator. This in turn produces a latitudinal entropy variation via equation (4) which spreads into the convection zone through turbulent diffusion and establishes non-cylindrical rotation profiles through baroclinic (thermally-induced) forcing.

The simulations considered here do not possess a subadiabatic tachocline. Thus, mechanical forcing such as imposing uniform rotation on the lower boundary would not promote thermal wind balance through induced circulations as in Rempel's (2005) model. Since we expect thermal wind balance to apply near the base of the convection zone, thermal forcing on the lower boundary may provide a more reliable means by which to account for the coupling between the convection zone and radiative interior via the tachocline. This is the motivation behind the present work.

The consequences of this thermal forcing are apparent in the results discussed in §3. The imposed entropy variation is transmitted throughout the convection zone by nonlinear advection (Fig. 3). This in turn induces a meridional circulation which establishes non-cylindrical

rotation profiles (Fig. 2) as described by equations (3) and (5). Since thermal wind balance is largely achieved (Fig. 5), the induced circulation ceases throughout most of the domain, leaving patterns similar to the unforced case. However, the stress-free boundary condition disrupts thermal wind balance and a residual circulation (clockwise in the northern hemisphere) remains in a thin boundary layer near the lower boundary (Fig. 6).

We emphasize that thermal wind balance near the base of the convection zone in our simulations is thermally-induced whereas in Rempel's (2005) mean-field model it is mechanically-induced. Thus, the induced circulations which establish this balance are opposite; respectively clockwise and counter-clockwise in the northern hemisphere as described by equation (3). We also emphasize that these circulations are transient; when thermal wind balance is approximately established, they cease. Other circulations driven by residual Coriolis forces, baroclinicity, Reynolds stresses and Lorentz forces, may persist beyond this adjustment phase.

In the Sun, thermal variations in the tachocline may arise by similar means. Helioseismic inversions indicate that a rotational shear is clearly present in the subadiabatic region below the convection zone. If this shear is maintained by mechanical forcing, a meridional circulation will be induced [cf. eqn. (3)] which will tend to warm the poles ($\partial \langle S \rangle / \partial \theta < 0$ in the northern hemisphere), moving the tachocline toward thermal wind balance. If there is an additional meridional circulation originating in the convection zone which flows into the subadiabatic tachocline at high latitudes and flows out at low latitudes then these thermal variations may be further enhanced. However, it should be noted that convection zone circulations which are not maintained by a persistent longitudinal forcing (gyroscopic pumping) would not penetrate deeper than the overshoot region (Gilman & Miesch 2004). Meanwhile, circulations which are maintained by gyroscopic pumping would continue to burrow downward into the radiative interior unless some mechanism were there to prevent it (Spiegel & Zahn 1992; Gough & McIntyre 1998). Thus, the resulting entropy structure, circulation patterns, and rotational shear are all intimately linked to tachocline confinement.

What is the nature of the mechanical forcing which maintains the tachocline? There is much debate on the details of this question but the overall picture is more widely accepted. Namely, turbulent stresses in the convection zone establish a latitudinal differential rotation while some process or combination of processes in the radiative interior keeps this differential rotation from spreading downward. A variety of mechanisms have been proposed, involving anisotropic turbulence, hydrodynamic and magneto-hydrodynamic shear instabilities, gravity waves and magnetic torques (Spiegel & Zahn 1992; Rüdiger & Kitchatinov 1997; Gilman & Fox 1997; Gough & McIntyre 1998; MacGregor & Charbonneau 1999; Talon et al. 2002; Forgács-Dajka & Petrovay 2002; Cally et al. 2003; Dikpati et al. 2003; Sule et al. 2005; Brun & Zahn 2005).

Whether the forcing is predominantly mechanical or thermal, and regardless of its physical nature, induced meridional circulations will tend to establish thermal wind balance in the subadiabatic portion of the tachocline wherever Reynolds stresses and Lorentz forces are negligible. In magnetic tachocline confinement models, Lorentz forces are not negligible in the lower tachocline but if the upper tachocline is relatively field-free, then thermal wind balance may still apply near the base of the convection zone.

5. CONCLUSIONS

The simulations presented in this paper demonstrate how sensitive the solar differential rotation may be to the thermal structure of the tachocline and overshoot region. We have found that imposing a weak entropy variation as the base of the convection zone can give rise to more solar-like (conical) angular velocity profiles. The relative amplitude of this imposed variation is of order 5×10^{-6}, corresponding to a pole-equator temperature difference of about 10K.

Dynamics near the base of the solar convection zone pose a formidable challenge to global convection simulations. High spatial and temporal resolution are required to reliably capture the relatively small-scale dynamics associated with convective overshoot, tachocline instabilities, internal waves, and other phenomena such as the magnetic boundary layers associated with some tachocline confinement models (e.g., Rüdiger & Kitchatinov 1997; Gough & McIntyre 1998). Explictly resolving all of these processes is beyond the capability of current models. If some aspects of these dynamics could be captured through appropriate boundary conditions imposed at the base of the convection zone it may provide new insight into convection zone dynamics. In this respect, the imposed latitudinal entropy variations considered here are justified and promising. However, they are not intended as an end in themselves; global simulations still must strive to explicitly resolve dynamics within the overshoot region and tachocline if they are to make further contact with helioseismic inversions and observations of magnetic activity.

Continuing advances in supercomputing are allowing simulations with progressively higher spatial resolution which can more faithfully capture the highly turbulent dynamics in the convection zone and overshoot region (Brun et al. 2005). We expect that momentum and heat transport from narrow downwelling plumes may alter as simulations achieve more turbulent parameter regimes, possibly yielding more solar-like rotation profiles as a result of altered turbulent transport. Thermal, magnetic, and mechanical coupling to the tachocline may reinforce the rotation profiles thus established.

The greatest realism in our models can only be achieved by explicitly resolving convective penetration into the radiative interior. However, steps can be taken short of this ultimate goal which could improve upon the non-penetrative models considered here. For example, the simulations here may be made more self-consistent by imposing a rotational shear on the lower boundary which is in thermal wind balance with the imposed entropy variation according to equation (1). Furthermore, the amplitude and form of this imposed shear and entropy variation should depend on the rotation profile achieved in the convection zone. For example, if there were a large $\Delta\Omega$ in the convection zone this would imply a large $\partial\Omega/\partial r$ across the tachocline. Thus, the rotation profile which is achieved should depend on feedback between turbulent stresses within the convection zone and

a dynamic lower boundary condition. We reserve these issues for future work.

In Rempel's (2005) mean-field approach, entropy gradients which originate from thermal wind balance in the tacholine are transmitted to the convection zone through turbulent thermal diffusion which is specified as part of his model. By contrast, the heat transport in our simulations is achieved via nonlinear advection by convective motions which are explicitly resolved. The striking result in both studies is that even weak latitudinal entropy variations attributed to processes in the tachocline can influence the Ω profiles achieved in the bulk of the convective envelope. Such effects can substantially improve the correspondence between dynamical models and helioseismic rotational inversions.

We thank Matthias Rempel for motivating this work and for comments on the manuscript and Peter Gilman and Jean-Paul Zahn for informative discussions. This work was partly supported by NASA through SEC Theory Program grants NAG5-11879 and NNG05G124G, and work orders W-10,177 and W-10,175. The supercomputer simulations were carried out with NSF PACI support of SDSC and PSC, as well as the CEA resource of CCRT and CNRS-IDRIS in France.

REFERENCES

Altrock, R. C. & Canfield, R. C. 1972, Solar Physics, 23, 257
Antia, H. M., Chitre, S. M., & Thompson, M. J. 2003, A&A, 399, 329
Basu, S. & Antia, H. M. 2003, ApJ, 585, 553
Bonnanno, A., Elstner, D., Belvedere, G., & Rüdiger, G. 2005, Astron. Nachr., 326, 170
Braun, D. C. & Fan, Y. 1998, ApJ, 508, L105
Brun, A. S., , DeRosa, M. L., Miesch, M. S., & Toomre, J. 2005, in preparation
Brun, A. S., Miesch, M. S., & Toomre, J. 2004, ApJ, 614, 1073
Brun, A. S. & Toomre, J. 2002, ApJ, 570, 865
Brun, A. S. & Zahn, J.-P. 2005, Magnetic Confinement of the Solar Tachocline, submitted
Cally, P. S., Dikpati, M., & Gilman, P. A. 2003, ApJ, 582, 1190
Charbonneau, P. 2005, Living Rev. Sol. Phys., 2, 1, (online journal) http://www.livingreviews.org/lrsp-2005-2
Charbonneau, P. & Dikpati, M. 2000, ApJ, 543, 1027
Clune, T. C., Elliott, J. R., Miesch, M. S., Toomre, J., & Glatzmaier, G. A. 1999, Parallel Computing, 25, 361
Dikpati, M. & Charbonneau, P. 1999, ApJ, 518, 508
Dikpati, M., de Toma, G., Gilman, P. A., Arge, C. N., & White, O. R. 2004, ApJ, 601, 1136
Dikpati, M., Gilman, P. A., & Rempel, M. 2003, ApJ, 596, 680
Durney, B. R. 1996a, Sol. Phys., 166, 231
—. 1996b, Sol. Phys., 169, 1
—. 1999, ApJ, 511, 945
—. 2001, Sol. Phys., 202, 201
Durney, B. R. & Spruit, H. C. 1979, ApJ, 234, 1067
Elliott, J. R., Miesch, M. S., & Toomre, J. 2000, ApJ, 533, 546
Forgács-Dajka, E. & Petrovay, K. 2002, A&A, 389, 629
Giles, P. M., Duvall, T. L., Scherrer, P. H., & Bogart, R. S. 1997, Nature, 390, 52
Gilman, P. A. 1968, Science, 169, 760
—. 1977, Geophys. Astrophys. Fluid Dyn., 8, 93
—. 1978, Geophys. Astrophys. Fluid Dyn., 11, 157
Gilman, P. A. & Fox, P. A. 1997, ApJ, 484, 439
Gilman, P. A. & Howe, R. 2003, in Local and Global Helioseismology: The Present and Future, ed. H. Sawaya-Lacoste, SP-517 (Noordwijk: ESA), 283–285
Gilman, P. A. & Miesch, M. S. 2004, ApJ, 611, 568
Gilman, P. A. & Miller, J. 1986, ApJS, 61, 585
Glatzmaier, G. A. 1984, J. Chem. Phys., 55, 461
Gough, D. O. & McIntyre, M. E. 1998, Nature, 394, 755
Haber, D. A., Hindman, B. W., Toomre, J., Bogart, R. S., Larsen, R. M., & Hill, F. 2002, ApJ, 570, 855
Hathaway, D. H. 1996, ApJ, 460, 1027
Jouve, L. & Brun, A. S. 2006, in preparation
Kitchatinov, L. L. & Rüdiger, G. 1995, A&A, 299, 446
—. 2005, Astron. Nachr., 326, 379
Kuhn, J. R., Libbrecht, K. G., & Dicke, R. H. 1988, Science, 242, 908
Küker, M., Rüdiger, G., & Schultz, M. 2001, A&A, 374, 301
Küker, M. & Stix, M. 2001, A&A, 366, 668
MacGregor, K. B. & Charbonneau, P. 1999, ApJ, 519, 911
McIntyre, M. E. 1998, Prog. Theor. Phys. Supl., 130, 137, corrigendum, Prog. Theor. Phys., 101, 189 (1999).
Miesch, M. S. 2005, Living Rev. Sol. Phys., 2, 1, (online journal) http://www.livingreviews.org/lrsp-2005-1
Miesch, M. S., Elliott, J. R., Toomre, J., Clune, T. C., Glatzmaier, G. A., & Gilman, P. A. 2000, ApJ, 532, 593
Nandy, D. & Choudhuri, A. R. 2002, Science, 296, 1671
Pedlosky, J. 1987, Geophysical Fluid Dynamics, 2nd edn. (New York: Springer-Verlag)
Plaskett, H. H. 1959, MNRAS, 119, 197
Rempel, M. 2005, ApJ, 622, 1320
Robinson, F. J. & Chan, K. L. 2001, MNRAS, 321, 723
Rüdiger, G., Egorov, P., Kitchatinov, L. L., & Küker, M. 2005, A&A, 431, 345
Rüdiger, G. & Hollerbach, R. 2004, The Magnetic Universe. Geophysical and Astrophysical Dynamo Theory (Weinheim: Wiley-VCH)
Rüdiger, G. & Kitchatinov, L. L. 1997, Astron. Nachr., 5, 273
Schou, J., Howe, R., Basu, S., Christensen-Dalsgaard, J., Corbard, T., Hill, F., Komm, R., Larsen, R. M., Rabello-Soares, M. C., & Thompson, M. J. 2002, ApJ, 567, 1234
Snodgrass, H. B. & Dailey, S. B. 1996, Solar Physics, 163, 21
Spiegel, E. A. & Zahn, J.-P. 1992, A&A, 265, 106
Sule, A., Rüdiger, G., & Arlt, R. 2005, A&A, 437, 1061
Talon, S., Kumar, P., & Zahn, J.-P. 2002, ApJ, 574, L175
Thompson, M. J., Christensen-Dalsgaard, J., Miesch, M. S., & Toomre, J. 2003, ARA&A, 41, 599
Weiss, N. O. 1965, Observatory, 85, 37
Woodard, M. F. & Libbrecht, K. G. 2003, Solar Physics, 212, 51
Zhao, J. & Kosovichev, A. G. 2004, ApJ, 603, 776